Supplementary Information

Ligand Specific Bioconjugation Induced Modulation of Quantum Yeild in CdTe and Graphene Quantum Dots

Akhil Khajuria[1#], Jatinder Kaur[1#], Hema K Alajangi[2#], Suraj Pratap Singh[2], Pritiman Pothal[1], Manpreet Singh[1], Mahima Thakur[1], *Pavitra Ranawat[2], *Ravi Pratap Barnwal[2] and *Gurpal Singh[1].

[1]*University Institute of Pharmaceutical Sciences, Panjab University, Chandigarh, India*

[2]*Department of Biophysics, Panjab University, Chandigarh, India*

Akhil Khajuria (akhilkhajuria16@gmail.com)
Jatinder Kaur (jatinderatwork92@gmail.com)
Hema K Alajangi (hemasai.biotech@gmail.com)
Suraj Pratap Singh (surajonenonly@gmail.com)
Pritiman Pothal (pritimanpothal@gmail.com)
Manpreet Singh (manpreet296416@gmail.com)
Mahima Thakur (mahimathakur282000@gmail.com)
Pavitra Ranawat (pavitraranawat@gmail.com)
Ravi Pratap Barnwal (barnwal@pu.ac.in)
Gurpal Singh (gurpalsingh.ips@gmail.com)

#Akhil Khajuria, Jatinder Kaur and Hema K Alajangi are equal contributors

***Corresponding Authors**: Pavitra Ranawat (pavitraranawat@gmail.com), Ravi Pratap Barnwal (barnwal@pu.ac.in), and Gurpal Singh (gurpalsingh.ips@gmail.com)

Materials:

DNA was procured from the Department of Biophysics at Punjab University, Chandigarh, India. Several reagents were obtained from TCI, Tokyo, Japan, including cadmium perchlorate hexahydrate, iron (III) chloride hexahydrate (97%), 1-(3-dimethylaminopropyl)-3-ethylcarbodiimide hydrochloride, and N-hydroxysuccinimide. Chemicals such as N,N-dimethylformamide, zinc telluride, 1,2-dichlorobenzene, 3-mercaptopropionic acid, and Rhodamine-6G were purchased from Sigma-Aldrich, USA. Additional reagents including potassium chloride, sodium chloride, sodium hydroxide, ethanol, hydrochloric acid, acetone, potassium hydrogen phosphate, hexane, thiamine hydrochloride, citric acid, and diethyl ether were supplied by Sisco Research Laboratories Pvt. Ltd., India.

Box S1: Advantages of aqueous synthesis method of CdTe QDs

- Simple and highly reproducible method
- Relatively economic process
- Smaller sized QDs are obtained
- Highly stable QDs are synthesized that can be stored as long as 2 years under ambient conditions
- Ease of controlling surface charge and other surface properties of QDs
- Safe reactants are used
- Environment-friendly process

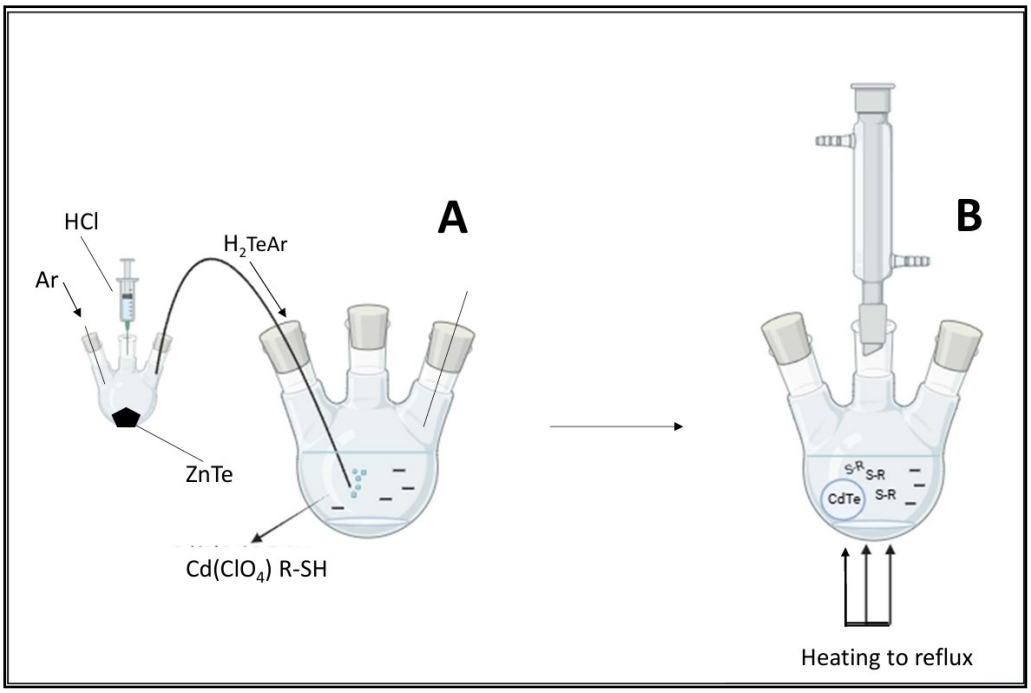

Supplementary Figure 1: Schematic illustration of the synthesis of thiol-capped CdTe QDs (I) formation of CdTe precursor by introducing H_2Te gas and (II) formation and growth of CdTe nanocrystals promoted by heating under reflux

Box S2: Advantages of the aqueous synthesis method of GQDs

- **Stable fluorescence properties**
- **Relatively economic process**
- **Smaller-sized QDs are obtained**
- **Produces GQDs with good dispersibility in aqueous solutions**
- **Ease of controlling surface charge and other surface properties of QDs**
- **Results in non-toxic GQDs suitable for biological applications.**
- **Environment-friendly process**

A. Determination of concentration

The concentration of CdTe-MPA QDs was assessed utilizing a PerkinElmer UV/VIS Spectrometer Lambda 35 for ultraviolet-visible (UV-Vis) spectrophotometry. The absorption spectra were obtained, and the concentration of CdTe-MPA QDs was determined using Beer-Lambert's law, as illustrated in Equation S1.

$A = \epsilon.C.L$ ……Equation S1

Where A denotes the sample's first exciton absorption peak, C is the sample's QDs' molar concentration (mol/L) and L is the length (in cm) of the path taken by the radiation beam as it

passes through the sample being used to capture the absorption spectrum. L was set to be 1 cm, ϵ is the extinction coefficient of QDs per mole (L/mol cm). Equation S2 was used to derive the extinction coefficient (ϵ) in equation S1.

CdTe: $\epsilon = 3450\ \Delta E(D)^{2.4}$ ….. Equation S2

Where ΔE ($\Delta E = 1240/\lambda_{max}$) is the transition energy corresponding to the first absorption peak and the unit is in eV. D is the diameter of the QDs and was calculated using equation S3.

CdTe: $D = (9.8127x10^{-7})\lambda^3 - (1.7147x10^{-3})\lambda^2 + (1.0064)\lambda - (194.84)$ …… Equation S3

Where λ (nm) is the wavelength of the first excitonic absorption peak of the QD sample. After getting values of Є and D from Equation S2 and S3, the concentration of CdTe QDs was calculated by Beer-lambert's law (Equation S1) [1].

S3: Methodology

S3.1 Determination of concentration

Table 4.1 illustrates the spectrophotometric absorbance (λ_{max}), band gap, particle size and concentration of CdTe-MPA QDs, and values were calculated from Equations S1 to S3 mentioned previously under the experimental section (S2).

Table S3: Concentration and size of various synthesized CdTe-MPA QDs batches

Sample	λ_{max}	Particle size (nm)	Band Gap (eV)	Concentration (mol/L)
CdTe 1	340	12.31	3.65	18.8×10^{-8}
CdTe 2	341	12.14	3.64	16.7×10^{-8}
CdTe 3	341	12.14	3.64	16.7×10^{-8}
CdTe 4	340	12.31	3.65	18.8×10^{-8}
CdTe 5	339	12.49	3.66	18.8×10^{-8}

It was observed that CdTe-MPA QDs prepared in different occasions (n=5) showed reproducible results. Their λ_{max} values ranged from 339 nm to 341 nm, absorbance values from 0.807 to 0.992, bandgap from 3.64 to 3.66 eV, and concentration ranging 167 to 188 nmol/L are shown in Table S3.

S3.2: Comprehensive Characterization of Synthesized CdTe-MPA QDs and GQDs

To ensure consistency and high coupling efficiency during the EDC/NHS-mediated reactions, all bioconjugations were carried out under carefully controlled physicochemical conditions. The reactions were performed **in the absence of light (dark conditions)** to prevent photochemical degradation of the reactive intermediates, **at a maintained temperature of 0–4 °C**, and **under continuous magnetic stirring** to ensure uniform dispersion and reaction

kinetics. A **phosphate buffer system (pH 7.4)** was employed to provide a physiologically relevant and stable environment for both the quantum dots and biomolecules. These standardized parameters consistently produced stable, monodisperse conjugates with strong fluorescence retention, demonstrating the reproducibility and reliability of the conjugation process. Following successful synthesis, CdTe-MPA QDs and GQDs were diluted tenfold in double-distilled water to facilitate their physicochemical and structural characterization. The hydrodynamic diameter, polydispersity index (PDI), and zeta potential were determined using dynamic light scattering (DLS) with a DelsaTM Nano C Particle Analyzer (Beckman Coulter, USA), yielding crucial information on their dispersion characteristics and colloidal stability. Optical properties were examined via a PerkinElmer Lambda 35 UV/VIS spectrophotometer and a Hitachi F-2500 fluorescence spectrophotometer, employing excitation wavelengths of 400 nm for CdTe-MPA QDs and 335 nm for GQDs. A concentration-dependent photoluminescence study was conducted to relate emission intensity to nanoparticle concentration, including assessments of both conjugated and unconjugated nanostructures. Morphological evaluation was performed using transmission electron microscopy (JEOL JEM-2100 at 200 kV), while crystal structure determination of lyophilized samples (CdTe-MPA QDs: 0.15–0.2 g; GQDs: 0.1 g) was done using powder X-ray diffraction (PXRD) with CuKα radiation (λ = 1.5406 Å, 45 kV, 40 mA). Scans were performed from 5° to 50° 2θ at 0.017° intervals and 25-second scan times. OriginPro 8 software was used for diffraction data analysis, focusing on identifying structural characteristics. Furthermore, functional group and bonding analyses were conducted via FTIR spectroscopy using the KBr pellet method in the 500–4500 cm^{-1} range on a Varian EM 360 instrument (60 MHz, PerkinElmer, USA), averaging 16 scans per sample. These investigations supported the assessment of ligand-induced alterations and vibrational features in both conjugated and non-conjugated QDs [2,3,4,5].

S4: Results and discussion

1. Characterization of CdTe-MPA QDs and GQDs

1.1. Dynamic light scattering (DLS) and zeta potential measurements

The effective size and size distribution of CdTe-MPA QDs and GQDs disseminated in water are illustrated in Supplementary Figure 2 (a and b). Based on the findings, it was seen that the QDs that were distributed in the water exhibited a much narrower size range. The average diameter of CdTe QDs was approximately 51.2 ± 21.7 nm, while the diameter of GQDs was approximately 120.9 nm. This finding is in line with the findings that have been published in the literature, namely in the years [8–10]. **Supplementary Figure 2 (c and d)** shows that CdTe-MPA QDs and GQDs have zeta potential of -21.7 ± 4.30 mV and -0.71mV, respectively. The presence of a negative charge on the surface of QDs is accountable for the stability of QDs. These negatively charged particles experience strong repulsive forces, which ultimately prevent particle aggregation [11].

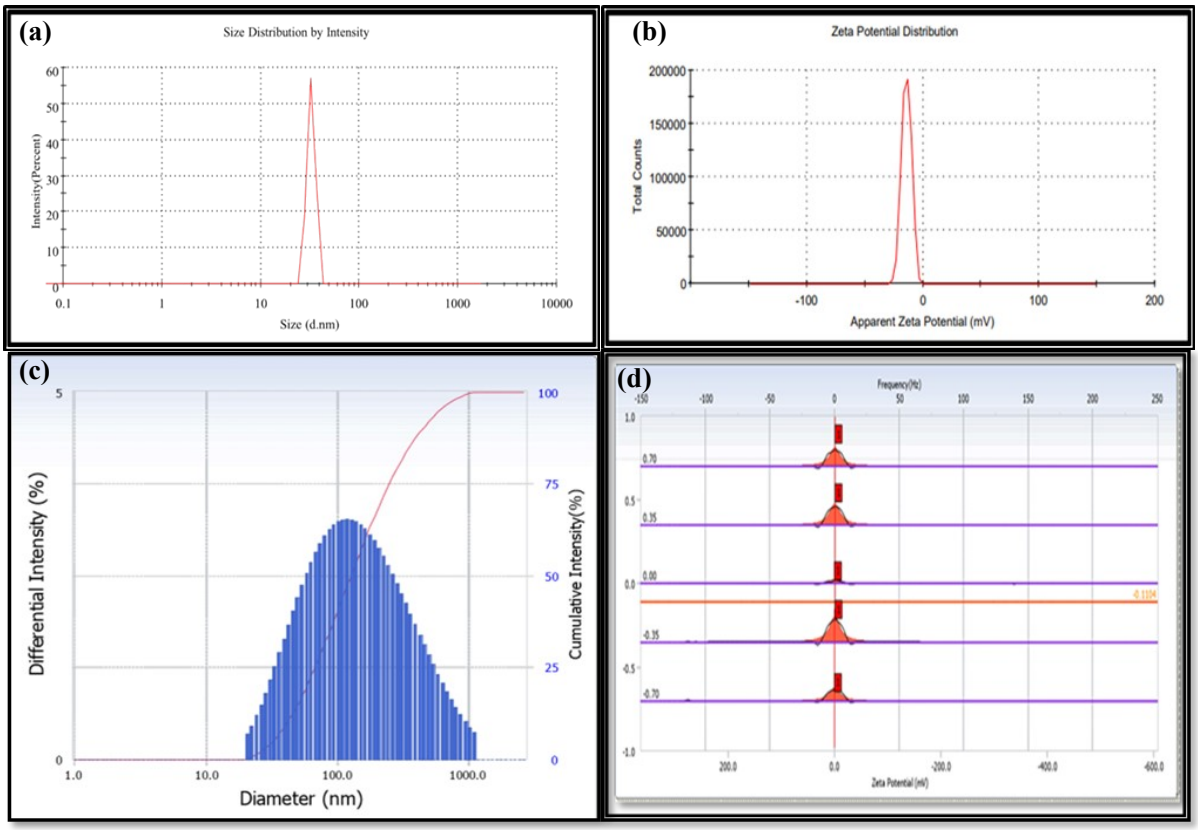

Supplementary Figure 2: (a) Particle size measurements of CdTe-MPA QDs (b) Zeta potential distribution of CdTe-MPA QDs (c) Particle size measurements of GQDs (d) Zeta potential distribution of GQD

2. Polydispersity index (PDI)

The PDI of the synthesized CdTe-MPA QDs and GQDs was found to be 0.272 ± 0.032 (n=1) and 0.320 (n=1) has been shown in **Supplementary Figure 3**, respectively, indicating that they are moderately polydisperse and possess a relatively uniform size profile [12,13].

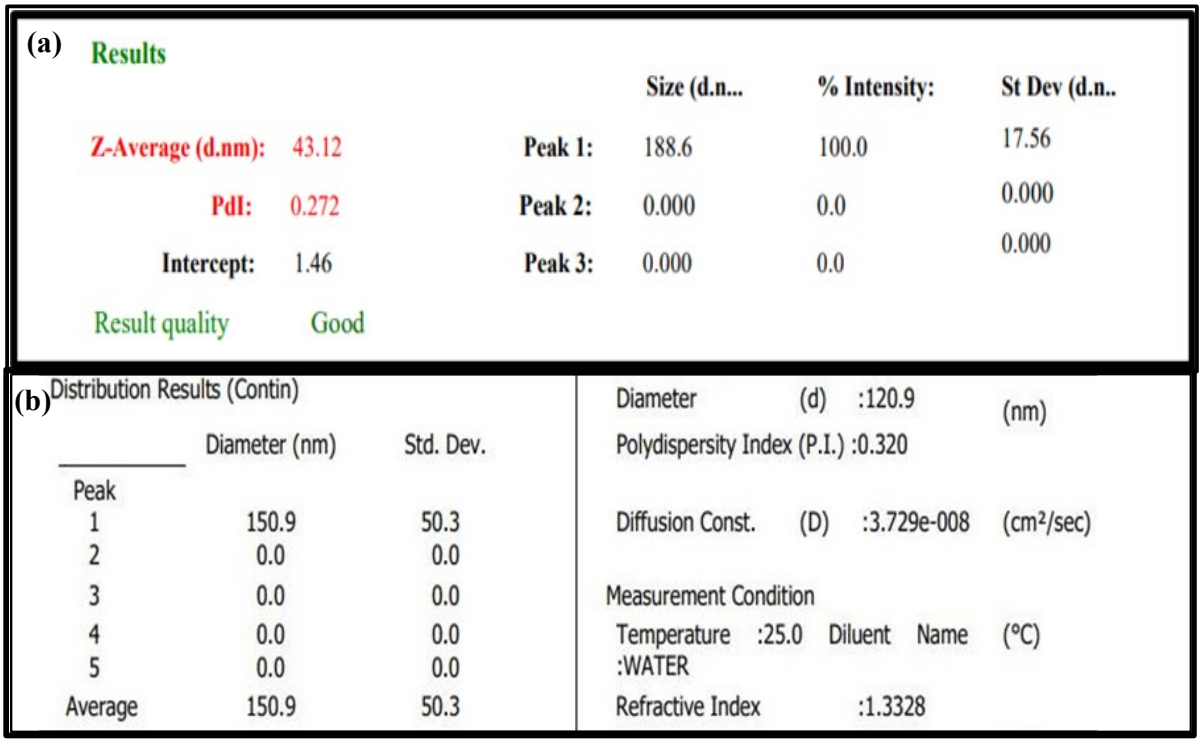

Supplementary Figure 3: (a) Polydispersity Index of CdTe-MPA QDs, (b) Polydispersity index of GQDs

3. Absorption and fluorescence spectroscopy

3.1 Absorption spectroscopy

As shown in **Supplementary Figure 4(a)**, CdTe quantum dots stabilized with MPA showed a maximum absorption at 340 nm when measured using a UV-visible spectrophotometer. Similarly, GQDs show UV-vis absorption maxima at 215 and 335 nm, as observed by a UV-visible spectrophotometer **Supplementary Figure 4 (b)**. Electronic transitions from C=O to π–π* transitions from C=C are corresponding to the peaks, which correspond to π-π* transitions. The peak observed at a wavelength of 335 nm is a result of electron transfer from n-π* through electronic transitions that include sp2 carbon structures originating from C=O. The peak at 215 nm, on the other hand, is due to π-π* transitions that happen with C=C bonds.

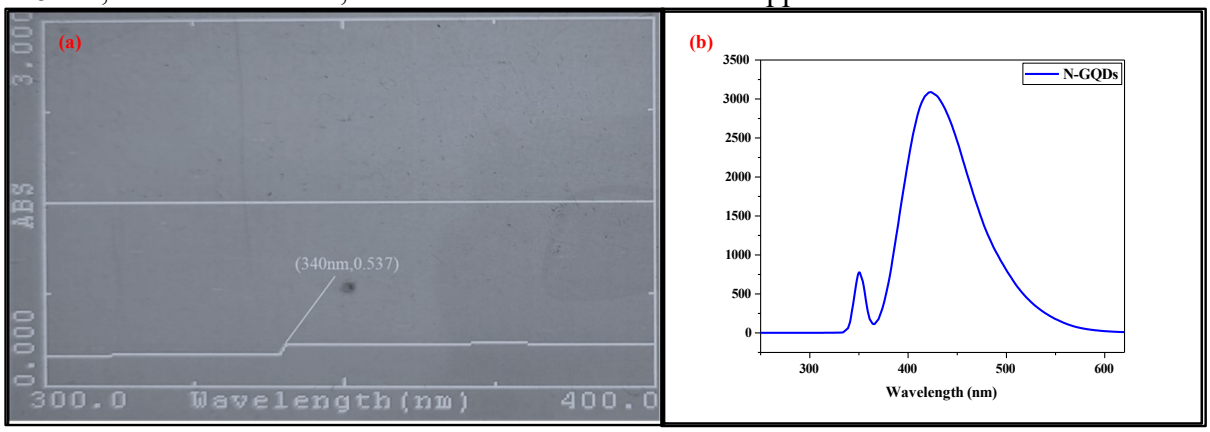

Supplementary Figure 4: (a) Absorbance Spectra of CdTe-MPA quantum dots and (b) GQD

S4.1 Powder X-ray diffraction (PXRD)

The XRD pattern of lyophilized CdTe-MPA QDs powder has peaks at 25°, 43°, and 50°, as shown in **Supplementary Figure 5 (a)**. These peaks correspond to (111), (220), and (311), respectively, which shows that the powder is crystalline [14,15]. Similarly, XRD measurements of the synthesized N- GQDs were used to verify the graphitic structure shown in **Supplementary Figure 5 (b)**. The diffraction peak for the GQDs appears at 2θ= 20°, possibly representing the turbostratic carbon phase and corresponding to the (002) plane with the d-spacing of 0.43 nm FTIR spectra confirming the functionalization of the synthesized GQDs.

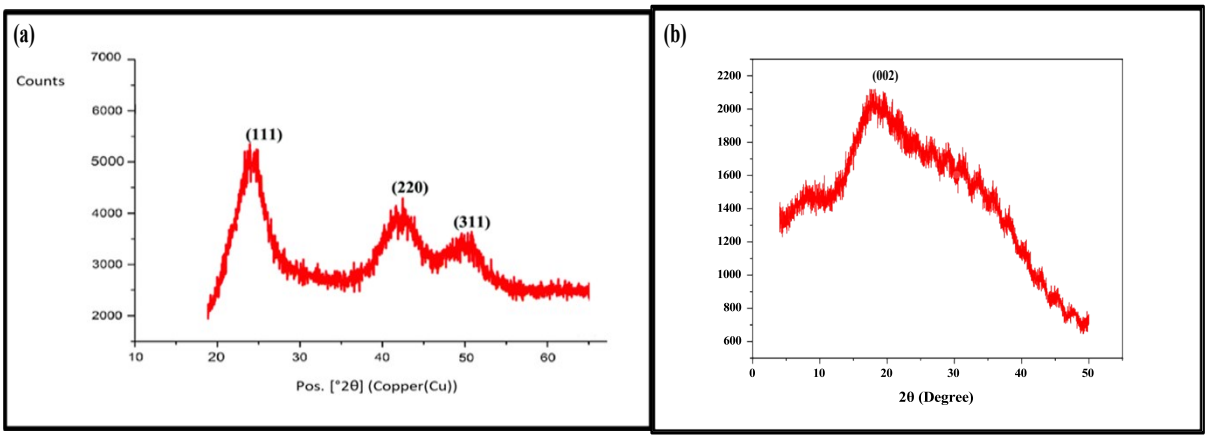

Supplementary Figure 5: (a) X-Ray diffraction pattern of CdTe-MPA QDs and (b) *GQDs*

S4.2. Fourier-transform infrared spectroscopy (FTIR)

Fourier-transform infrared (FTIR) spectroscopy was utilized to identify the functional groups present on the surface of quantum dots (QDs), serving as a reliable method for structural characterization. For CdTe-MPA QDs, the IR spectrum displayed peaks at 1401 cm^{-1} and 1561 cm^{-1}, representing symmetric and asymmetric stretches of the carboxylate (–COO–) group, respectively. A broad absorption above 3000 cm^{-1} was attributed to –OH stretching from –COOH groups, while a smaller band at 2935 cm^{-1} indicated CH_2 vibrations. The 1087 cm^{-1} peak confirmed the presence of –C–O bonds from carboxylic acids, supporting stabilization via MPA. Absence of the –SH stretching peak at 2574 cm^{-1} further verified effective capping by MPA ligands. In the case of nitrogen-doped GQDs (N-GQDs), the FTIR spectrum exhibited a broad band around 3400 cm^{-1} corresponding to O–H and possible N–H stretching, indicating nitrogen incorporation. Peaks at 1630 cm^{-1} and 1380 cm^{-1} were assigned to C=C/C=O and N–O stretching vibrations, respectively, confirming the presence of aromatic, carboxylic, and nitrogen-containing functional groups. These findings indicate enhanced water dispersibility, stability, and successful nitrogen doping of GQDs due to the identified surface functionalities[16].

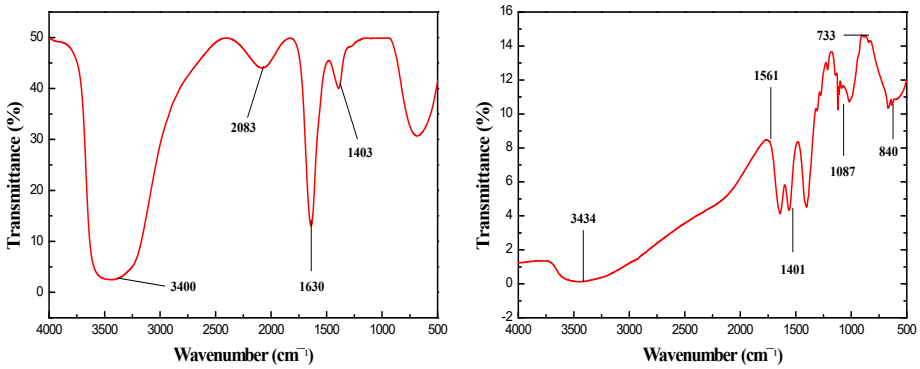

Supplementary Figure 6: (a) FTIR spectra of CdTe-MPA QDs and (b) GQDs

S4.3 High-resolution transmission electron microscopy (HR-TEM)

Supplementary Figure 7 (a and b) shows HR-TEM images of CdTe-MPA QDs, which reveal that the spherical-shaped QDs are monodispersed and have a particle size of around 5.0 to 6.0 nm. Also, these QDs, which were all the same shape, were found to be very far apart from each other [17]. **Supplementary Figures 7 (c and d)** show HR-TEM images of N-doped GQDs, indicating NP distribution across the field. The crystalline structure of these particles is composed of a single or a few layers of graphene. N-GQDs have a size that is relatively consistent, with an average size of approximately 2.3 nm.

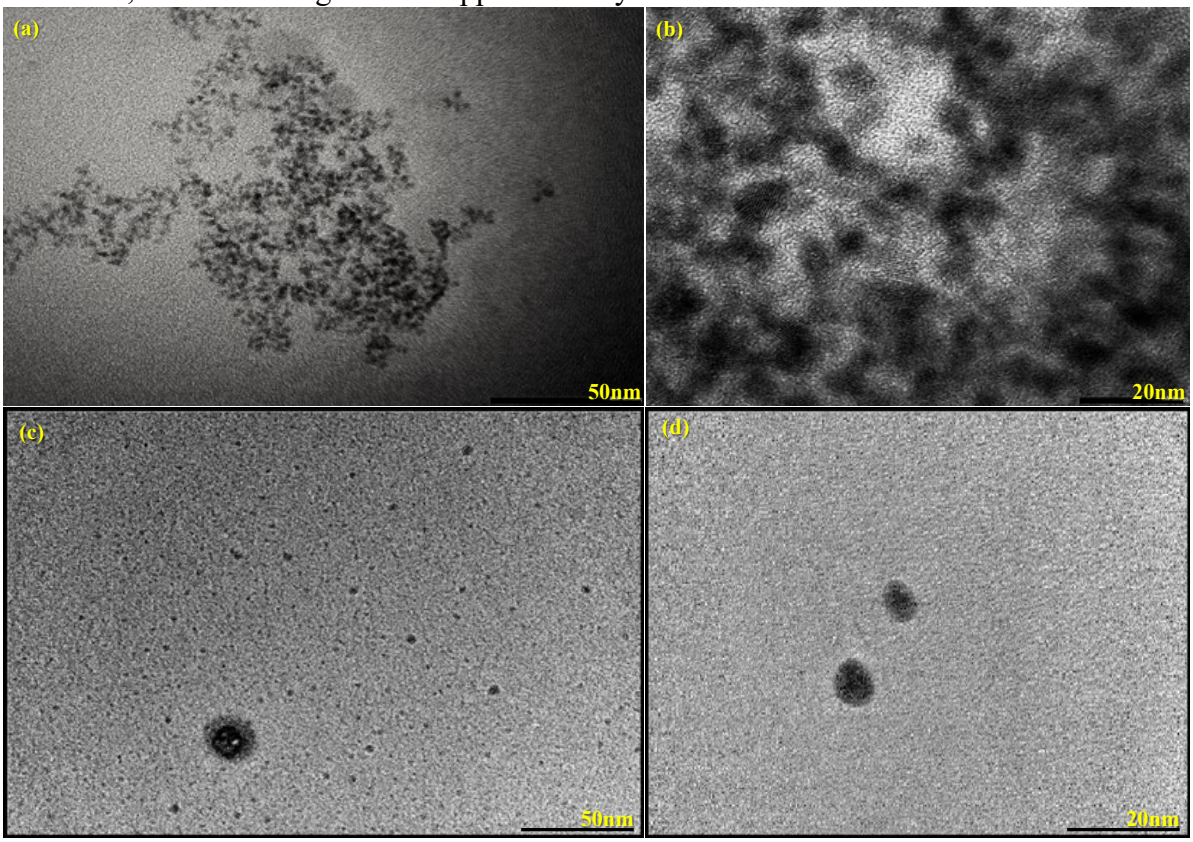

Supplementary Figure 7: (a and b) HR-TEM images of CdTe-MPA QDs and (c and d) GQDs

References:

1 N. T. Vo, H. D. Ngo, D. L. Vu, A. P. Duong and Q. V. Lam, *J Nanomater*, DOI:10.1155/2015/265315.

2 A. M. Smith, H. Duan, A. M. Mohs and S. Nie, *Adv Drug Deliv Rev*, 2008, **60**, 1226–1240.

3 C. Zhang, Y. Zhou, L. Tang, G. Zeng, J. Zhang, B. Peng, X. Xie, C. Lai, B. Long and J. Zhu, *Nanomaterials*, 2016, **6**, 1–11.

4 C. Wang, X. Cui, Y. Li, H. Li, L. Huang, J. Bi, J. Luo, L. Q. Ma, W. Zhou, Y. Cao, B. Wang and F. Miao, *Sci Rep*, DOI:10.1038/SREP21711.

5 M. Abdulla, A. Ali, R. Jamal, T. Bakri, W. Wu and T. Abdiryim, *Polymers (Basel)*, DOI:10.3390/POLYM11050815.

6 R. ; D. A. ; R. S. M. ; G. T. ; Z. Y. ; K. S. ; K. M. J. ; G. Y. N. ; E. A. ; C. Y. J. ; M. A. V. Bose, R. Bose, A. Dangerfield, S. M. Rupich, T. Guo, Y. Zheng, S. Kwon, M. J. Kim, Y. N. Gartstein, A. Esteve, Y. J. Chabal and A. V. Malko, *ACS Appl Nano Mater*, 2018, **1**, 6782–6789.

7 A. Bose, I. Thomas and E. Abraham, *International Journal of Advances in Pharmaceutical Analysis*, DOI:10.7439/ijapa.

8 A. Arivarasan, G. Sasikala and R. Jayavel, *Mater Sci Semicond Process*, 2014, **25**, 238–243.

9 G. Singh, M. Kumar, U. Soni, V. Arora, V. Bansal, D. Gupta, M. Bhat, A. K. Dinda, S. Sapra and H. Singh, *J Nanosci Nanotechnol*, 2016, **16**, 130–143.

10 A. Pant, T. Kaur, T. Sharma, J. Singh, A. Suttee, R. Pratap Barnwal, I. Pal Kaur, G. Singh and B. Singh, .

11 Z. Mamipour, M. Kompany-Zareh and A. Nematollahzadeh, *Analytical Methods*, 2023, **15**, 6073–6081.

12 A. Arivarasan, G. Sasikala and R. Jayavel, *Mater Sci Semicond Process*, 2014, **25**, 238–243.

13 M. Shen, W. Jia, Y. You, Y. Hu, F. Li, S. Tian, J. Li, Y. Jin and D. Han, *Nanoscale Res Lett*, 2013, **8**, 253.

14 Z. Nguqu, O. A. Daramola and F. B. Dejene, *Results Chem*, 2025, **15**, 102214.

15 H. N. Noori and A. F. Abdulameer, *Chemical Methodologies*, 2022, **6**, 842–850.

16 B. Zhang, P. Zou, J. Li, D. Lu, X. J. Wang and L. Ma, *ACS Appl Nano Mater*, 2022, **5**, 4677–4687.

17 C. Wang, X. Cui, Y. Li, H. Li, L. Huang, J. Bi, J. Luo, L. Q. Ma, W. Zhou, Y. Cao, B. Wang and F. Miao, *Sci Rep*, 2016, **6**, 1–8.